



# WALLABY Pilot Survey: HI in the Host Galaxy of a Fast Radio Burst

M. Glowacki<sup>1</sup>, K. Lee-Waddell<sup>1,2,3</sup>, A. T. Deller<sup>4</sup>, N. Deg<sup>5</sup>, A. C. Gordon<sup>6</sup>, J. A. Grundy<sup>1,3</sup>, L. Marnoch<sup>7,8,9,10</sup>, A. X. Shen<sup>3</sup>, S. D. Ryder<sup>7,8</sup>, R. M. Shannon<sup>4</sup>, O. I. Wong<sup>2,3,10</sup>, H. Dénes<sup>11</sup>, B. S. Koribalski<sup>12,13</sup>, C. Murugesan<sup>3,10</sup>, J. Rhee<sup>2,10</sup>, T. Westmeier<sup>2,10</sup>, S. Bhandari<sup>9,11,14,15</sup>, A. Bosma<sup>16</sup>, B. W. Holwerda<sup>17</sup>, and J. X. Prochaska<sup>18,19,20</sup>

<sup>1</sup>International Centre for Radio Astronomy Research (ICRAR), Curtin University, Bentley, WA 6102, Australia; [marcin.glowacki@curtin.edu.au](mailto:marcin.glowacki@curtin.edu.au)

<sup>2</sup>International Centre for Radio Astronomy Research (ICRAR), The University of Western Australia, 35 Stirling Hwy, Crawley, WA 6009, Australia

<sup>3</sup>CSIRO Space and Astronomy, P.O. Box 1130, Bentley, WA 6102, Australia

<sup>4</sup>Centre for Astrophysics and Supercomputing, Swinburne University of Technology, Hawthorn, VIC 3122, Australia

<sup>5</sup>Department of Physics, Engineering Physics, and Astronomy, Queen's University, Kingston, ON K7L 3N6, Canada

<sup>6</sup>Center for Interdisciplinary Exploration and Research in Astrophysics and Department of Physics and Astronomy, Northwestern University, 2145 Sheridan Road, Evanston, IL 60208-3112, USA

<sup>7</sup>School of Mathematical and Physical Sciences, Macquarie University, NSW 2109, Australia

<sup>8</sup>Astronomy, Astrophysics and Astrophotonics Research Centre, Macquarie University, Sydney, NSW 2109, Australia

<sup>9</sup>CSIRO, Space and Astronomy, P.O. Box 76, Epping NSW 1710 Australia

<sup>10</sup>ARC Centre of Excellence for All Sky Astrophysics in 3 Dimensions (ASTRO 3D), Australia

<sup>11</sup>ASTRON, Netherlands Institute for Radio Astronomy, Oude Hoogeveensedk 4, 7991 PD Dwingeloo, The Netherlands

<sup>12</sup>CSIRO Astronomy and Space Science, Australia Telescope National Facility, P.O. Box 76, NSW 1710, Australia

<sup>13</sup>School of Science, Western Sydney University, Locked Bag 1797, Penrith, NSW 2751, Australia

<sup>14</sup>Joint Institute for VLBI ERIC, Oude Hoogeveensedk 4, 7991 PD Dwingeloo, The Netherlands

<sup>15</sup>Anton Pannekoek Institute for Astronomy, University of Amsterdam, Science Park 904, 1098 XH, Amsterdam, The Netherlands

<sup>16</sup>Aix Marseille Univ, CNRS, CNES, LAM, Marseille, France

<sup>17</sup>University of Louisville, Department of Physics and Astronomy, Natural Science Building 102, Louisville, KY 40292, USA

<sup>18</sup>Department of Astronomy and Astrophysics, University of California, Santa Cruz, CA 95064, USA

<sup>19</sup>Kavli Institute for the Physics and Mathematics of the Universe, 5-1-5 Kashiwanoha, Kashiwa 277-8583, Japan

Received 2022 October 25; revised 2023 February 27; accepted 2023 March 5; published 2023 May 24

## Abstract

We report on the commensal ASKAP detection of a fast radio burst (FRB), FRB 20211127I, and the detection of neutral hydrogen (HI) emission in the FRB host galaxy, WALLABY J131913–185018 (hereafter W13–18). This collaboration between the CRAFT and WALLABY survey teams marks the fifth, and most distant, FRB host galaxy detected in HI, not including the Milky Way. We find that W13–18 has an HI mass of  $M_{\text{HI}} = 6.5 \times 10^9 M_{\odot}$ , an HI-to-stellar mass ratio of 2.17, and coincides with a continuum radio source of flux density at 1.4 GHz of 1.3 mJy. The HI global spectrum of W13–18 appears to be asymmetric, albeit the HI observation has a low signal-to-noise ratio (S/N), and the galaxy itself appears modestly undisturbed. These properties are compared to the early literature of HI emission detected in other FRB hosts to date, where either the HI global spectra were strongly asymmetric, or there were clearly disrupted HI intensity map distributions. W13–18 lacks a sufficient S/N to determine whether it is significantly less asymmetric in its HI distribution than previous examples of FRB host galaxies. However, there are no strong signs of a major interaction in the optical image of the host galaxy that would stimulate a burst of star formation and hence the production of putative FRB progenitors related to massive stars and their compact remnants.

*Unified Astronomy Thesaurus concepts:* [H I line emission \(690\)](#); [Radio transient sources \(2008\)](#); [Galaxy mergers \(608\)](#)

## 1. Introduction

To date, we do not know the origin of fast radio bursts (FRBs; Lorimer et al. 2007), the highly energetic radio pulses occurring on timescales of milliseconds and found to originate at extragalactic distances. While several theories exist (see the review by Cordes & Chatterjee 2019), this is an ongoing area of debate. To address this issue best, we need to identify and dissect the host galaxies of FRBs better, through localization of their radio signals. One of the main aims of the Commensal Real-time ASKAP Fast Transients survey (CRAFT; Macquart et al. 2010; Bannister et al. 2017) is to localize FRBs at

subarcsecond scales with the Australian Square Kilometre Array Pathfinder telescope (ASKAP; Deboer et al. 2009). Dedicated follow-up observations (e.g., at optical wavelengths) of these localized FRB positions give us important information to categorize the host galaxies and better understand the possible mechanisms behind FRBs (Bhandari et al. 2022).

Stellar information alone does not inform us on the gas content and distribution, from which stars form and can lead to FRB progenitors. One way to map the gas distribution is through the neutral hydrogen (HI) 21 cm transition with radio telescopes. The HI spatial distribution and kinematics can constrain the recent history of a galaxy. Since HI gas often extends beyond the stellar distribution, we can also better see the indicators of recent galaxy interactions, such as tidal tails and extensions (Holwerda et al. 2011; Reynolds et al. 2019). Such features may be difficult to detect in optical studies, but can be prominent in HI intensity maps and velocity fields. Another possible indicator of galaxy interactions can be seen

<sup>20</sup> Simons Pivot Fellow.

**Table 1**  
Summary of Other H I Emission Detections for FRB Host Galaxies

| FRB Name      | Host Galaxy     | Redshift | Notes on H I Content and Host Galaxy                                                                                                                                                                                                                                                           |
|---------------|-----------------|----------|------------------------------------------------------------------------------------------------------------------------------------------------------------------------------------------------------------------------------------------------------------------------------------------------|
| FRB 20171020A | ESO 601–G036    | 0.008672 | Lee-Waddell et al. (2023). The host galaxy has a faint stellar companion and a tidal tail visible in the H I intensity map and a lopsided H I global spectrum. Both features are attributed to a galaxy interaction event.                                                                     |
| FRB 20180916B | SDSS J0158+6542 | 0.03399  | Kaur et al. (2022) presented a disturbed H I distribution from intensity and velocity maps, and concluded this galaxy is merging.                                                                                                                                                              |
| FRB 20181030A | NGC 3252        | 0.0038   | Michałowski (2021) found the H I global spectrum from Masters et al. (2014) to be strongly asymmetric relative to the general galaxy population and GRB hosts.                                                                                                                                 |
| FRB 20200120E | M81             | 0.00014  | M81 is the dominant galaxy of the M81/M82/NGC 3077 group. The data in Chynoweth et al. (2008) show a complex structure of the overall H I distribution in this group, and the global spectrum of M81 by itself is strongly asymmetric relative to the general galaxy population and GRB hosts. |
| FRB 20200428  | Milky Way       | ...      | The asymmetric H I distribution is covered in the review by Kalberla & Kerp (2009). Interacting with the Large Magellanic Cloud and Small Magellanic Cloud.                                                                                                                                    |

**Note.** Each host galaxy was concluded to have had a recent (or ongoing) galaxy merger or interaction event.

in asymmetries of the H I global spectrum (e.g., Deg et al. 2020).

Thus far, many identified FRB host galaxies show evidence of star formation and would hence be expected to contain H I. However H I emission has only been detected in four FRB host galaxies, outside of the Milky Way, due to the current limited number ( $<30$ ) of localized FRBs and the large distances to their hosts limiting the ability to detect H I emission directly (the median redshift of localized FRB hosts used in James et al. 2022 is  $z = 0.237$ ). In Table 1, we summarize these galaxies with H I emission detections. With the issues arising from low number statistics in mind, one early trend that has emerged is that all of these host galaxies were claimed to have strongly asymmetric 21 cm spectra or highly disturbed H I distributions. Michałowski (2021) highlights that the two published FRB host galaxies at the time that were known to have H I emission—not including the Galactic magnetar in the Milky Way—had highly asymmetric H I global spectra, to a far greater degree than what is typically seen for the general galaxy population or hosts of long-duration gamma-ray bursts (GRBs). While the H I global spectrum analyzed by Michałowski (2021) for one FRB host is of the M81 group, Figure 2 of Chynoweth et al. (2008) showcases the strongly asymmetric spectrum for M81 in isolation. We also note that the Masters et al. (2014) spectrum of NGC 3252 analyzed by Michałowski (2021) includes a baseline ripple. Our Milky Way is currently interacting with other systems e.g., the Large and Small Magellanic Clouds. Recently, Kaur et al. (2022) reported a Giant Metrewave Radio Telescope (GMRT) detection of H I in the host galaxy of the repeating FRB 20180916B. They found that the H I distribution was highly disturbed, the source had two tidal tails, and there was a clear H I deficit between the center of the galaxy and FRB location. Additionally, Lee-Waddell et al. (2023), using data from the Australia Telescope Compact Array, showed that the identified host galaxy of FRB 20171020A (Mahony et al. 2018) has an asymmetric H I global spectrum and a clear H I tail. Hsu et al. (2023) recently presented asymmetric profiles of molecular gas (CO) in the host galaxy of FRB 20180924B, and proposed FRBs could commonly appear in kinematically disturbed environments.

In all of these studies, the cause of the H I global spectrum asymmetry or disturbed H I distribution has been attributed to ongoing or recent galaxy interaction events. The tidal activity enhances star formation in the host, which supports “fast FRB

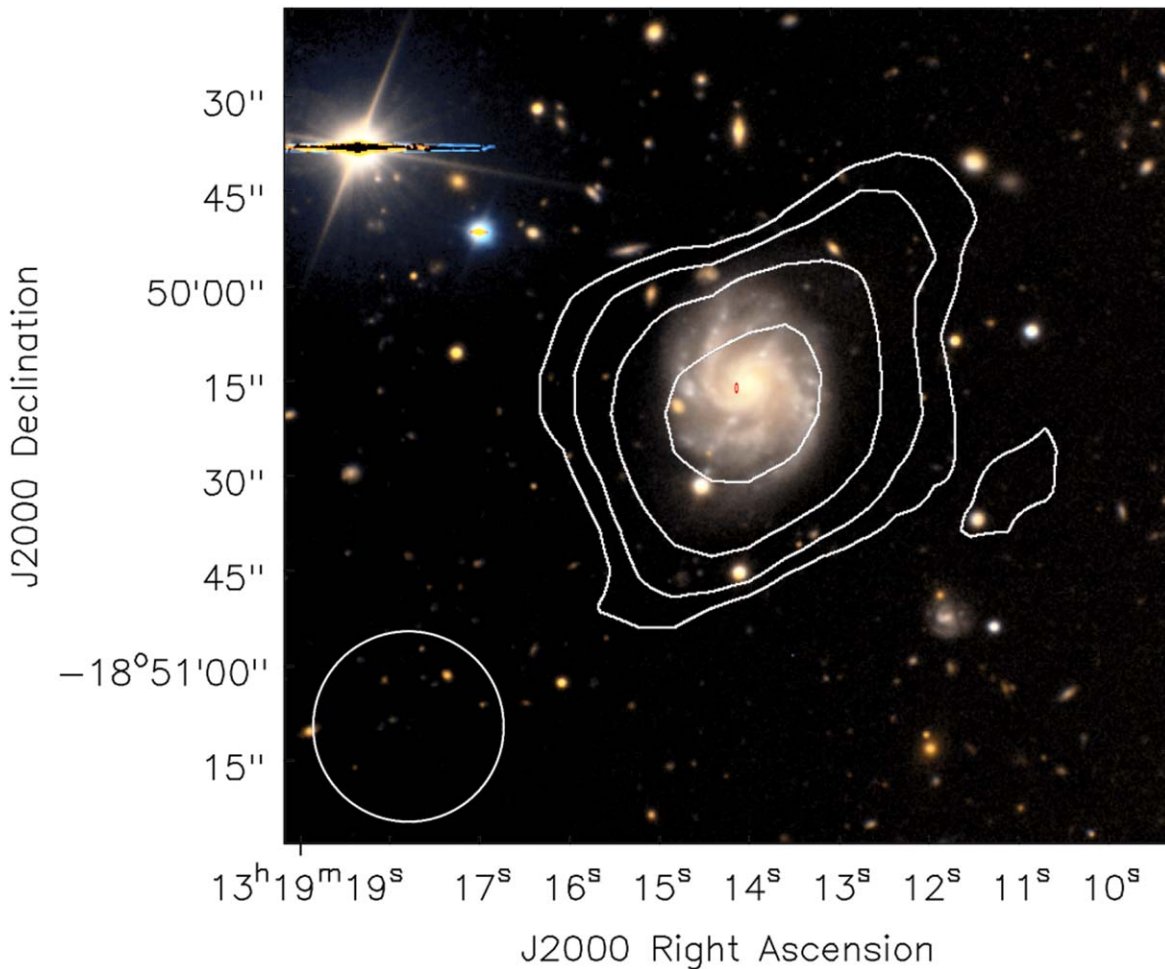
channels” (Michałowski 2021), i.e., a massive star collapsing in a supernova explosion into a magnetar with a short delay time acting as the FRB progenitor (as theorized for the FRB studied in Kaur et al. 2022). However, the current sample size is small and the statistics must be significantly improved to understand the FRB progenitor environment better. Is it possible that a massive star as the FRB progenitor could be created without the need for galaxy interaction, e.g., simply within a spiral galaxy arm? Will this trend persist for all FRB host galaxies observed in H I or is the story more complicated?

In this paper, we report on the H I content of one of these FRB hosts, FRB 20211127I, as derived from commensal ASKAP observations of the Widefield ASKAP L-band Legacy All-sky Blind survey (WALLABY; Koribalski et al. 2020) Pilot Survey Phase 2. During these observations, FRB 20211127I was detected by the CRAFT survey and subsequently localized to a nearby galaxy. In Section 2, we describe the WALLABY observations and source finding process. Section 3.1 presents an analysis of the H I properties. We compare with the existing literature of H I in FRB host galaxies in Section 3.2 and summarize our conclusions in Section 4.

## 2. Data

### 2.1. ASKAP Observations

The original WALLABY observations of regions in the vicinity of the NGC 5044 galaxy group were taken in late 2021 November and spanned a frequency range of 1151.5–1439.5 MHz. These observations had been affected by technical issues in the calibration data and could not be used for spectral line imaging. However, as part of the commensal observing strategy of CRAFT, an FRB was successfully detected with a signal-to-noise ratio (S/N) of 38 on 2021 November 27 UT 00:00:10, and localized to J2000 13:19:14.08,  $-18:50:16.7$ , with an estimated uncertainty of  $0''.2$  in R.A. and  $0''.8$  in decl. The localization made use of the astrometric pipeline initially described in Bannister et al. (2019) and extended in Day et al. (2020); see also Scott et al. (2023). The S/N of the FRB in the postprocessed image was 73, meaning that the positional uncertainty is dominated by the accuracy with which the systematic offsets can be estimated and removed using background radio sources detected in an image of the field made using the 3.1 s of voltage data (A. T. Deller et al. 2023, in preparation). This source was found to be coincident



**Figure 1.** H I intensity (moment 0) contour map of W13–18, from the SoFiA source finding output with contour levels shown at  $0.6$ ,  $1.2$ ,  $2.4$ , and  $4.8 \times 10^{20}$  atoms  $\text{cm}^{-2}$ , overlaid on a VLT  $g$ -band and  $I$ -band image (the rms of the WALLABY observation corresponds to  $0.2 \times 10^{20}$  atoms  $\text{cm}^{-2}$ ). The narrow red ellipse marks the localized position of FRB 202111271 (A. T. Deller et al. 2023, in preparation). The ASKAP synthesized beam (with spatial resolution =  $30''$ ) is indicated by the white ellipse in the lower left.

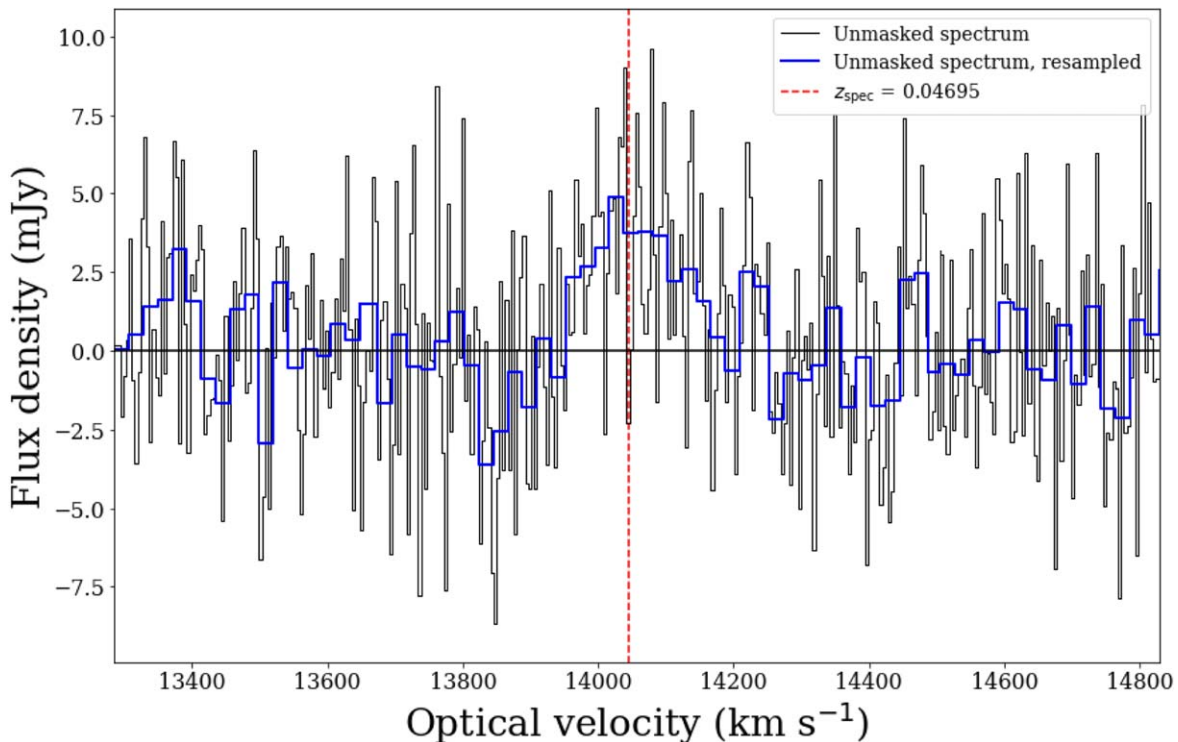
with the galaxy WISEA J131913.96–185016.2 (also known as 6dFGS gJ131914.0–185017, WALLABY J131913–185018, and hereafter W13–18), with a redshift  $z = 0.0469$  (Jones et al. 2009) that is consistent with the dispersion measure (DM) of  $227 \text{ pc cm}^{-3}$  found via the Macquart Relation (Macquart et al. 2020). Additional optical follow up of the FRB site and its host galaxy using  $g$ - and  $I$ -band imaging was performed with the FORS2 instrument mounted on Unit Telescope 1 (UT1) of the European Southern Observatory’s Very Large Telescope (VLT). These data were reduced using standard pipelines to produce the images shown in Figure 1; further analysis will be forthcoming in A. T. Deller et al. (2023, in preparation).

After the calibration issues on ASKAP were rectified, the same regions, which included W13–18, were reobserved in early 2021 December, under scheduling block (SB) IDs 34167 and 34278, as part of Pilot Phase 2 WALLABY observations. These data were edited, calibrated, and imaged using the automated ASKAPsoft processing pipeline (version 1.6.2; Whiting 2020) and standard WALLABY processing parameters. Observations and data reduction were as described for the Phase 1 Pilot Survey (Westmeier et al. 2022). In short, the observations included 15,552 spectral channels across the frequency range of 1151.5–1439.5 MHz, with only the upper 144 MHz retained due to radio frequency interference (RFI)

below 1300 MHz. Continuum emission was subtracted from the visibility data through a sky model derived from the calibrated and deconvolved continuum image, and imaging performed with a robust weighting of 0.5. Further continuum subtraction was then performed in the image domain. The multiscale CLEAN algorithm was used for deconvolution. The one difference for Phase 2 data processing is using holography constrained beams for the primary beam correction, rather than circular Gaussian beams, for more accurate image fluxes.

Each night of observations comprised one 36-beam footprint that was processed individually. Resulting data products are publicly available on the CSIRO ASKAP Science Data Archive (CASDA; Huynh et al. 2020) under the associated SBIDs. The image products for the corresponding footprints (i.e., footprints A and B with a common tile name) were mosaicked together to produce the final full sensitivity images and cubes. The combined WALLABY spectral line cube—imaged using ASKAP baselines up to 2 km—has a  $30''$  synthesized beam,  $\sim 4 \text{ km s}^{-1}$  spectral resolution, and an rms of  $\sim 1.6 \text{ mJy beam}^{-1}$  per channel in the region around W13–18. We note this is the idealized rms value for central beams in ASKAP’s field of view. The combined continuum map—imaged using all ASKAP baselines—has a  $9''$  resolution and an rms of  $20\text{--}30 \mu\text{Jy beam}^{-1}$ .





**Figure 2.** H I global spectrum for W13–18 in the heliocentric reference frame. The raw H I spectrum is given in black, and a resampled spectrum by a factor of 5 in blue. The optical spectroscopic redshift is indicated in red.

Source finding was carried out using the Source Finding Application 2 (SoFiA 2; Serra et al. 2015; Westmeier et al. 2021) through a custom pipeline developed by the Australian SKA Regional Centre (AusSRC), with a minimum S/N threshold of 3. Westmeier et al. (2022) provides a detailed description of the process used for WALLABY. W13–18 was identified, from the pipelined source finding, with a central position offset by  $0''.32$  and  $2''.8$  from the optical position of WISEA J131913.96–185016.2 (Jarrett et al. 2000) in R.A. and decl. respectively, consistent with the expected WALLABY centroid errors.

### 3. Results and Discussion

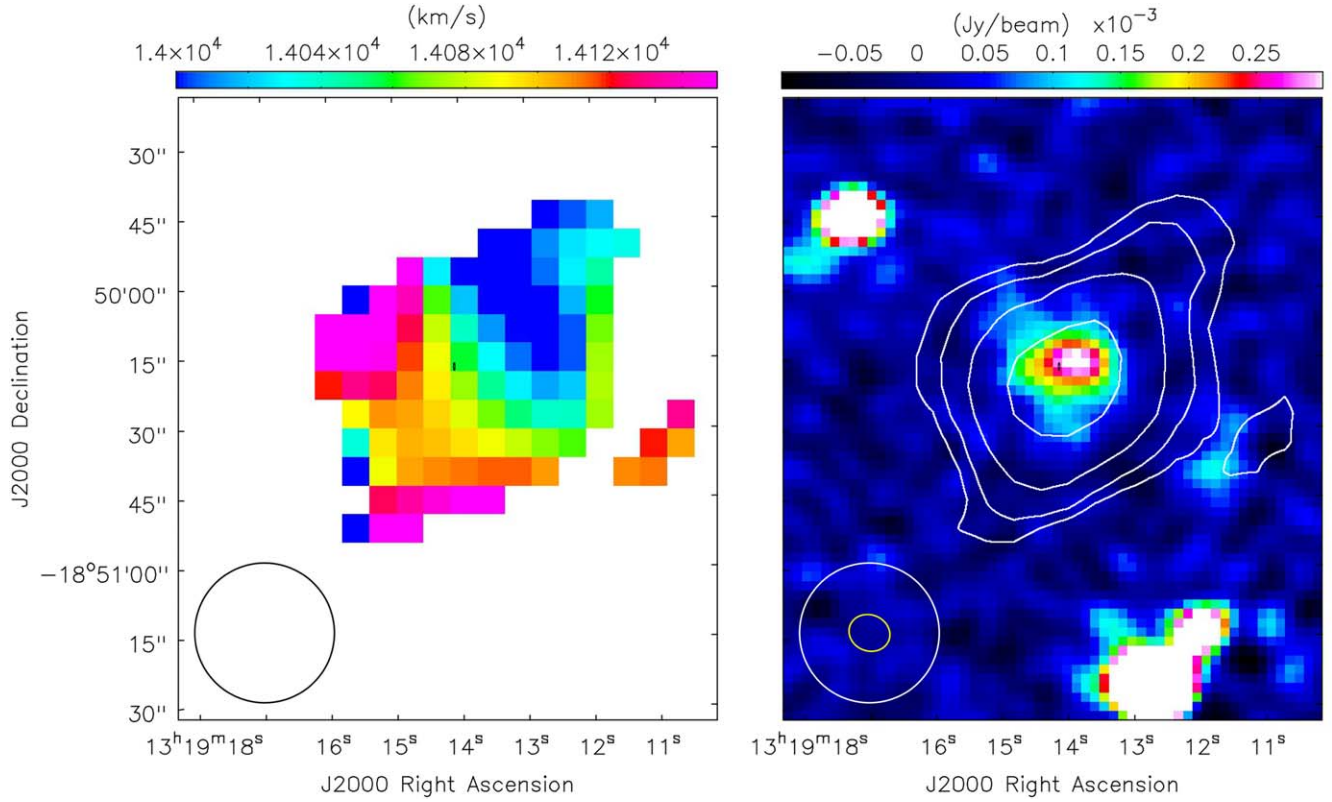
#### 3.1. H I and Stellar Properties

In Figure 1 we present the intensity map for W13–18, displayed as contours overlaid on the VLT image of the FRB host galaxy. The false color image used the VLT/FORS2 *g*-band for blue, VLT/FORS2 *I*-band for red, and an average of the two optical band images for green, which were combined through Astropy’s “make\_lupton\_rgb” function. The FRB localization at 68% confidence is overlaid as a red ellipse. Figure 2 shows the H I global spectrum of the host galaxy, from the raw spectral cube, including a version at lower spectral resolution by resampling the spectrum by a factor of 5. We also investigated a SoFiA-masked spectrum that was Hanning smoothed by a factor of 5. The velocity resolution of the raw spectrum of the host galaxy is  $4.28 \text{ km s}^{-1}$ . In Figure 3 we display the intensity map contours overlaid on the velocity map (left panel), and the radio continuum map (right panel). We do not detect any other H I sources along the line of sight to the galaxy in the SoFiA search, nor within the vicinity of the FRB signal. The H I mass sensitivity of the WALLABY observation following Equation (157) of Meyer et al. (2017), assuming an

S/N of 5, velocity width of  $200 \text{ km s}^{-1}$ , rms of  $1.6 \text{ mJy}$  per channel per beam, and an unresolved H I galaxy, is  $M_{\text{HIlim}} = 2.4 \times 10^9 M_{\odot}$ . The H I mass sensitivity is lower near the edges of the footprints.

We summarize the following properties calculated from the H I data and ancillary data in Table 2. Using the optical redshift of  $z = 0.04695$  (Jones et al. 2009; the corresponding distance is 215 Mpc assuming a Planck-constrained cosmology and  $H_0 = 67.7 \text{ km s}^{-1} \text{ Mpc}^{-1}$ ; Planck Collaboration et al. 2016), we find  $M_{\text{HI}} = 6.5 \pm 1.3 \times 10^9 M_{\odot}$ , where we include an assumed 5% calibration error for WALLABY in addition to the measured noise ( $\pm 1.0 \times 10^9 M_{\odot}$ ). Using *griz* photometry and spectroscopy from the Southern Astrophysical Research (SOAR) Telescope (PI Gordon, program SOAR2022B-007), *YJKs* photometry from VISTA (McMahon et al. 2013), and W1–W4 photometry from WISE (Wright et al. 2010), Gordon et al. (2023) determine a spectral energy distribution (SED)-derived stellar mass for W13–18 of  $3.0 \times 10^9 M_{\odot}$  ( $\log(M_*/M_{\odot}) = 9.48^{+0.02}_{-0.01}$ ). This value was calculated using the Bayesian stellar population synthesis code *Prospector* (Johnson et al. 2021). Further details on the data collection, reduction, assumed priors, and additional stellar population parameters for this galaxy are reported in Gordon et al. (2023). Our H I-to-stellar mass ratio is hence  $f_{\text{HI}} = M_{\text{HI}}/M_* \sim 2.17$  ( $\log$  ratio of 0.34), higher than the 1.3 ratio found for the FRB host studied by Kaur et al. (2022).

We attempt to estimate the total dynamical mass,  $M_{\text{dyn}}$ , of W13–18, using Equation (2) of Lee-Waddell et al. (2016). However, due to the low spatial resolution and S/N, we are unable to obtain a reliable estimate. In order to obtain an improved mass estimate, we attempted to kinematically model this galaxy using both 3D-Based Analysis of Rotating Objects From Line Observations (3DBAROLO; Di Teodoro & Fraternali 2015) and a modified version of the WALLABY Kinematic Analysis Proto-Pipeline (WKAPP; Deg et al. 2022).



**Figure 3.** Left panel: H I velocity (moment 1) map that has been masked using the lowest contour level ( $0.6 \times 10^{20}$  atoms  $\text{cm}^{-2}$ ) of the moment 0 map. Right panel: H I moment 0 contours (same levels as Figure 1) overlaid on the radio continuum. The  $9''$  continuum beam, which is at higher resolution than the spectral line cube due to the inclusion of all ASKAP baselines during imaging, is indicated by the smaller yellow ellipse in the bottom left of the right panel. Both panels show the FRB localized position.

**Table 2**

Measured Properties of W13–18 in Order of H I flux, H I Mass, W50 (with Error Measured from Generating Synthetic Spectra by Perturbing Each Channel by the Noise; See Section 3.2), Stellar Mass, Radio Continuum Flux, Total Global SFR from the Radio Continuum (Total and After Subtracting Unresolved Core Emission), SFR from WISE mid-infrared Photometry, the SFR of the Last 30 Myr Measured from the Prospector SED model, the SFR from GALEX NUV photometry, 1D Asymmetry Measurements (Lopsidedness and Residual of the Integrated Spectrum), and the 2D Asymmetry Measure

| Quantity                            | Value                                                                     |
|-------------------------------------|---------------------------------------------------------------------------|
| $S_{\text{H I}}$                    | $0.63 \pm 0.1 \text{ Jy km s}^{-1}$                                       |
| $M_{\text{H I}}$                    | $6.5 \pm 1.3 \times 10^9 M_{\odot}$                                       |
| W50                                 | $150 \pm 19 \text{ km s}^{-1}$                                            |
| $M_*$                               | $3.0 \pm 0.1 \times 10^9 M_{\odot}$                                       |
| $S_{1.37}$                          | 1.3 mJy                                                                   |
| $\text{SFR}_{\text{radio}}$         | $2.91^{+1.70}_{-1.07} \text{ }^{+0.05}_{-0.05} M_{\odot} \text{ yr}^{-1}$ |
| $\text{SFR}_{\text{radio no core}}$ | $1.77^{+1.04}_{-0.66} \text{ }^{+0.07}_{-0.07} M_{\odot} \text{ yr}^{-1}$ |
| $\text{SFR}_{\text{WISE}}$          | $2.57 \pm 0.28 M_{\odot} \text{ yr}^{-1}$                                 |
| $\text{SFR}_{\text{SED}}$           | $0.45^{+0.59}_{-0.36} M_{\odot} \text{ yr}^{-1}$                          |
| $\text{SFR}_{\text{UV}}$            | $1.22 \pm 0.05 M_{\odot} \text{ yr}^{-1}$                                 |
| $A_{\text{flux}}$                   | $1.12 \pm 0.13$                                                           |
| $A_{\text{spec}}$                   | $0.296 \pm 0.091$                                                         |
| $A_{2D}$                            | 0.23                                                                      |

Unfortunately the low spatial resolution and S/N precludes such sophisticated modeling. As shown in Deg et al. (2022), kinematic modeling of WALLABY detections even with full 3D codes requires  $\text{ell}_{\text{maj}} \geq 2$  beams and  $\log(\text{S/N}) \geq 1.25$ , and this detection satisfies neither requirement.

A radio continuum source with a flux density of 1.3 mJy is associated with the stellar disk at  $\sim 5\sigma$  significance. The flux-weighted center of the continuum source, determined through ProFound (Hale et al. 2019), is 13:19:14.06,  $-18:50:16.0$ . The angular separation between this source and the FRB localization is within the image resolution of the synthesized beam ( $9''$ ). Using the ASKAP spectral width at the 50% flux level of the masked spectrum (W50) of  $150 \text{ km s}^{-1}$ , we estimate the rotation curve amplitude ( $V_{\text{max}}$ ) to be  $\sim 100 \text{ km s}^{-1}$  after correcting for relativistic effects and expected turbulence broadening following Meyer et al. (2008), and also correcting for inclination ( $19.8^\circ$  from 2MASS) following Meurer et al. (2006). We find this  $V_{\text{max}}$  to be consistent with the stellar mass estimate for the host galaxy (Wong et al. 2016).

We follow the method described in Grundy 2023 applied to WALLABY galaxies to estimate the total global star formation rate (SFR) from the radio continuum. Using the relationship from Molnár et al. (2021) calibrated against the far-infrared (FIR)–radio correlation:

$$\log_{10} \left( \frac{\text{SFR}_{1.4}}{M_{\odot} \text{ yr}^{-1}} \right) = (0.823 \pm 0.009) \log_{10} \left( \frac{L_{1.4}}{\text{W Hz}^{-1}} \right) + 17.5 \pm 0.2, \quad (1)$$

we find the SFR to be  $2.91^{+1.70}_{-1.07} \text{ }^{+0.05}_{-0.05} M_{\odot} \text{ yr}^{-1}$ . While the WALLABY continuum value is not quite at 1.4 GHz (1.3675 GHz), in the Eridanus prepilot WALLABY field the flux values for unresolved, isolated sources are consistent with NVSS at 1.4 GHz within the scatter, so we use the WALLABY

fluxes without correction. As the origin of the central continuum emission could be due to star formation or a radio-quiet active galactic nucleus (AGN), we also estimate the total SFR beyond the host galaxy core (after subtracting the unresolved core emission) to be  $1.77_{-0.66}^{+1.04} {}_{-0.07}^{+0.07} M_{\odot} \text{ yr}^{-1}$ . We present both estimates as it is currently unclear whether the FRB relates to a star-forming region within the core or the inner spiral arm of this host galaxy. The first and second set of uncertainties are, respectively, the systematic and measured uncertainties for each SFR estimate.

The WISE colors of  $W1 - W2 = 0.10 \pm 0.29$  mag and  $W2 - W3 = 3.47 \pm 0.28$  mag suggest that W13–18 is unlikely to host a highly efficient accreting AGN as it fits among the normal star-forming spiral region of the WISE color–color diagram. As in Grundy 2023, we calculate the integrated WISE W3PAH (polycyclic aromatic hydrocarbon) SFR, following the relationship given in Cluver et al. (2014):

$$\begin{aligned} & \log_{10} \left( \frac{\text{SFR}_{\text{W3PAH}}}{M_{\odot} \text{ yr}^{-1}} \right) \\ &= 1.13 \log_{10} \left( v_{\text{W3}} \frac{L_{\text{W3PAH}}}{L_{\odot}} \right) - 10.24, \end{aligned} \quad (2)$$

calibrated against  $\text{H}\alpha$  observations. The WISE W3PAH is calculated by subtracting 15.8% of the total WISE W1 flux from the WISE W3 flux (both measured by ProFound) to account for the contribution of the evolved stellar population to the W3 flux, as in Jarrett et al. (2011), Cluver et al. (2017), and references therein. We find the WISE  $\text{SFR}_{\text{W3PAH}} = 2.57 \pm 0.28 M_{\odot} \text{ yr}^{-1}$ , which agrees well with the radio continuum SFR.

The GALEX near-UV (NUV) magnitude is 17.7345 mag. Converting this to a NUV luminosity, we then use Equation (6) of Schiminovich et al. (2007):

$$\text{SFR}_{\text{NUV}} (M_{\odot} \text{ yr}^{-1}) = 10^{-28.165} L_{\nu} (\text{erg s}^{-1} \text{ Hz}^{-1}), \quad (3)$$

and find an  $\text{SFR}_{\text{NUV}}$  of  $1.22 \pm 0.05 M_{\odot} \text{ yr}^{-1}$ .

The radio continuum SFR and  $M_{\text{HI}}$  estimates imply that the star formation efficiency (SFE) is  $\log(\text{SFE}_{\text{HI}}) = -10.2 {}_{-0.70}^{+0.36} \text{ yr}^{-1}$ , where  $\text{SFE}_{\text{HI}}$  is simply  $\text{SFR}/M_{\text{HI}}$ . This  $\text{SFE}_{\text{HI}}$  is consistent with the scatter of  $\text{SFE}_{\text{HI}}$  in the sample of HI-selected star-forming disk galaxies studied by Wong et al. (2016), who argued that the constant global  $\text{SFE}_{\text{HI}}$  observed for star-forming disk galaxies across five orders of stellar mass magnitude can be described by self-regulation in a constant, marginally stable disk.

From the Prospector SED model, the present-day SFR for W13–18 is  $0.45 {}_{-0.36}^{+0.59} M_{\odot} \text{ yr}^{-1}$  (Gordon et al. 2023). This value describes the SFR of the last 30 Myr, which is sensitive to the youngest stars in the galaxy. Gordon et al. (2023) finds that a starburst event may have occurred  $\sim 100$  Myr ago in W13–18. The optically derived specific SFR (sSFR) is  $\sim 1.5 \times 10^{-10} \text{ yr}^{-1}$  (log value of  $-9.82$ ). Considering both Table 1 and Figure 6 of Catinella et al. (2018)’s analysis of the extended Galaxy Evolution Explorer (GALEX) Arecibo Sloan Digital Sky Survey (SDSS) Survey (xGASS), as done in Figure 2 of Kaur et al. (2022), W13–18 is gas rich for galaxies in the mass bin of  $\log M_{*} = 9.44$ . The xGASS weighted average of the logarithmic gas fraction is  $-0.459 \pm 0.067$ , which is lower than the value we find for W13–18 of 0.34 (at the top of the scatter for xGASS). W13–18 also lies above the  $\log(M_{\text{HI}}/M_{*}) - \log(\text{sSFR}/\text{yr}^{-1})$  relation as the  $\log(\text{sSFR})$  bin of  $-9.72$  has a corresponding log

mass ratio of  $-0.063 \pm 0.041$ . The galaxy studied in Kaur et al. (2022) was further above the envelope of the xGASS distribution compared to where W13–18 would lie, at a similar sSFR (Figure 4). The gas richness of both galaxies may indicate that both FRB hosts recently acquired a large amount of HI. Relative to xGASS, W13–18 lies on the star-forming main sequence when considering the optical SFR for the last 30 Myr, or slightly above it when using the total WISE SFR (without subtracting core emission).

### 3.2. Investigating the Early Trend of Strong Asymmetry and Disturbed HI

As discussed in Section 1, other FRB host galaxies found to contain HI gas have shown an early trend: strongly asymmetric HI global spectra and/or disturbed intensity maps indicating these host galaxies are undergoing, or have recently undergone, merger/interaction events. It has been hypothesized that certain merger activity could result in a burst of star formation that in turn could create an FRB progenitor. In these scenarios, the FRB progenitor would be a massive star (Kaur et al. 2022) originating from a fast FRB channel model (Michałowski 2021).

For the host galaxy of FRB 202111271, we are limited by the S/N and spatial resolution to state confidently whether this remains the case. The HI intensity map for W13–18 (Figure 1) is fairly featureless and far less disturbed than the HI map of SDSS J0158+6542 presented in Kaur et al. (2022), albeit the available spatial resolution is low. The only unusual detail is a possible feature to the south west traced by the lower contour of  $0.6 \times 10^{20} \text{ atoms cm}^{-2}$ , with three possibilities. One is that this HI feature is associated with a nearby dwarf galaxy; however, there is no associated source in the optical data, and only nearby faint radio continuum emission.

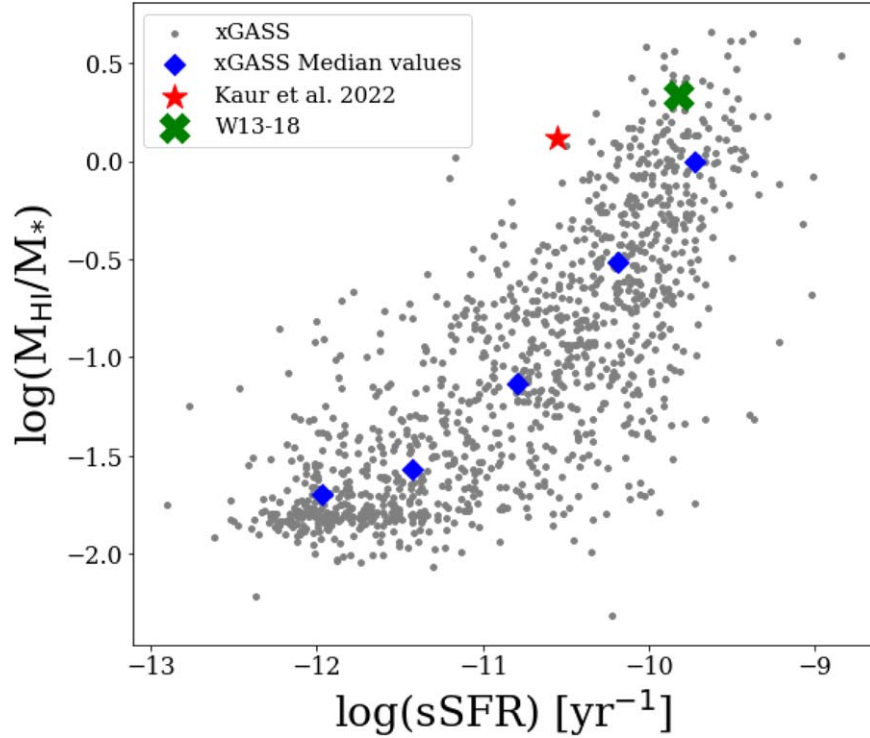
The second possibility is the feature is part of a tidal tail connected to the main emission, but the spatial resolution is not sufficient to confirm this notion. Furthermore, this feature is on the opposite side of the galaxy from the FRB localization and would likely not contribute to any enhanced star formation at the FRB source. The third and most likely possibility is that this feature is noise, especially considering its level of significance.

The only indication of any galaxy interaction is a very faint stellar overdensity extending to northwest of the galaxy in the VLT optical image, which appears to correspond with the extension in the HI intensity map. The overall position angle and inclination of the HI in W13–18 does not appear to be aligned with the stellar spiral structure; however, higher spatial resolution HI observations at greater sensitivity are required for a more detailed analysis.

The HI global spectrum has a higher amount of flux on the left hand (approaching) side. In order to compare best the level of its asymmetry with FRB hosts studied in Michałowski (2021), we adopt the same asymmetry measurement definitions used in that study and the values from Reynolds et al. (2020), for both the masked and unmasked resampled spectra (bottom panel of Figure 2). The ratio of the integrated flux in the left and right halves of the spectrum is (see also, e.g., Richter & Sancisi 1994; Haynes et al. 1998; Espada et al. 2011):

$$A_{\text{flux}} = |F_l/F_r|, \quad (4)$$





**Figure 4.** The H I-to-stellar mass ratio, plotted against sSFR, for xGASS galaxies given by the gray points with median values given in blue diamonds (Catinella et al. 2018), the FRB host studied by Kaur et al. (2022; SDSS J0158+6542; red star), and W13–18 (green cross). Both W13–18 and SDSS J0158+6542 have higher H I-to-stellar mass ratios, albeit SDSS J0158+6542 is notably higher than galaxies with comparable sSFR measures to itself.

where:

$$F_l = \int_{\nu_l}^{\nu_{\text{sys}}} F(\nu) d\nu, \quad (5)$$

and:

$$F_h = \int_{\nu_{\text{sys}}}^{\nu_r} F(\nu) d\nu, \quad (6)$$

where  $\nu_{\text{sys}}$  is the systemic velocity defined as the midpoint of the spectrum at the 20% flux level (i.e., the  $W_{20}$  line width), and  $\nu_l$  and  $\nu_r$  are, respectively, the left- and right-hand optical velocities where the flux density drops to 20% of the peak flux density. We also adopt Equation (8) of Reynolds et al. (2020) for the residual of the integrated spectrum that was found to have the most significant trend with local galaxy density. Simultaneously, Deg et al. (2020) found the residual of the integrated spectrum to be the best indicator for visually classified asymmetries, as employed in Glowacki et al. (2022). The integrated spectrum residual is defined as:

$$A_{\text{spec}} = \frac{\sum_{i=1} |S(i) - S_{\text{flip}}(i)|}{\sum_{i=1} |S(i)|}, \quad (7)$$

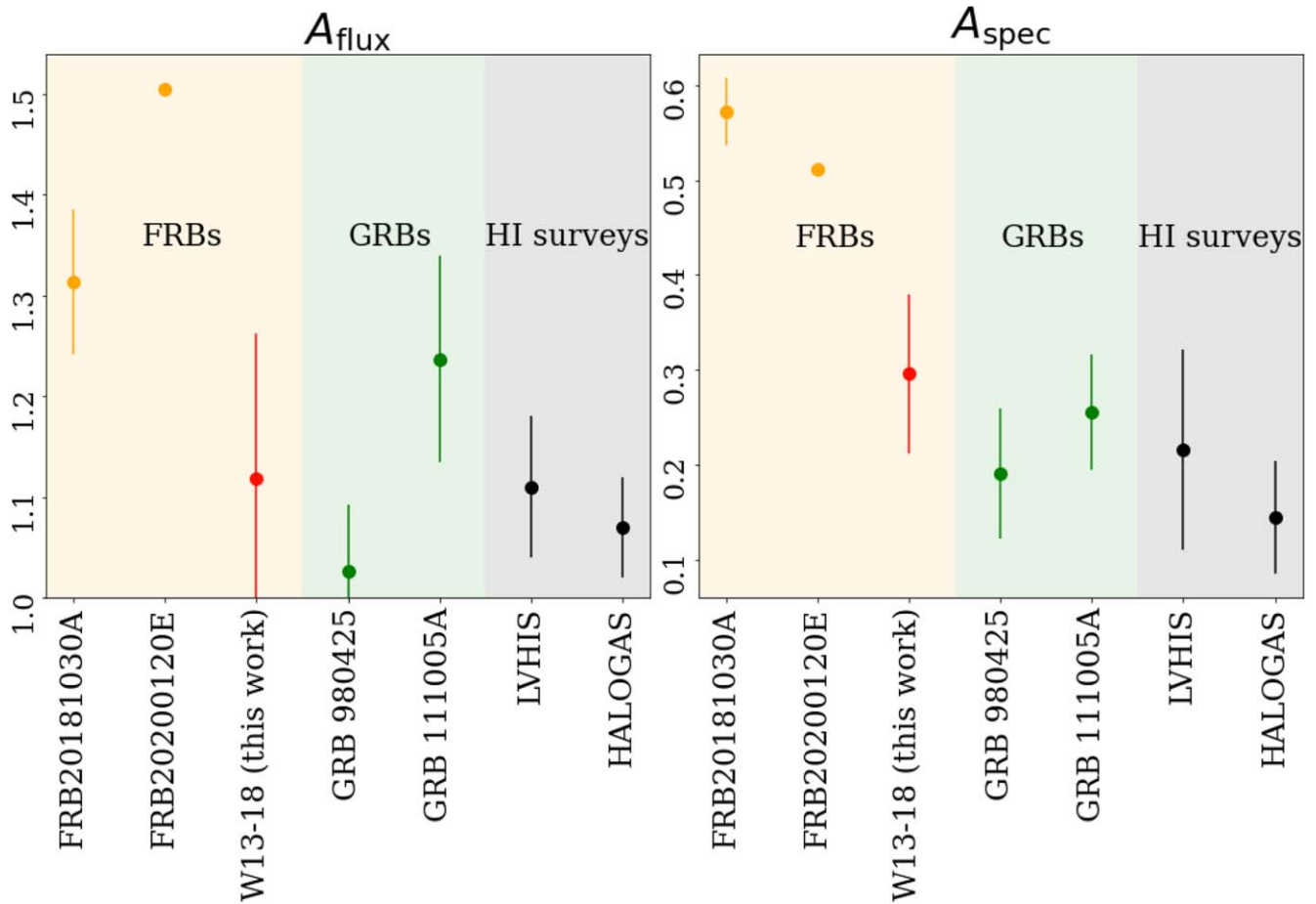
where  $S(i)$  and  $S_{\text{flip}}(i)$  are, respectively, the fluxes in channel  $i$  of the original and flipped spectrum, with the flip axis being the flux-weighted mean systemic velocity. We estimate the error in  $A_{\text{flux}}$  and  $A_{\text{spec}}$  in the same way as in Michałowski (2021): we construct a Gaussian distribution using the standard deviation of line-free channels as the width, and perturbed each channel in the spectrum 1000 times by a value drawn from this Gaussian distribution. The standard deviation of the asymmetry

measures of these synthetic spectra was taken as the uncertainty.

Michałowski (2021) found  $A_{\text{flux}}$  values of  $1.314 \pm 0.072$  and  $1.505 \pm 0.002$ , and  $A_{\text{spec}}$  values of  $0.5719 \pm 0.0351$  and  $0.5108 \pm 0.0005$  (see Table 1 of their study), significantly greater than the values found in Reynolds et al. (2020) for the Local Volume H I Survey (LVHIS; Koribalski et al. 2018) and the Hydrogen Accretion in Local Galaxies Survey (HALOGAS; Heald et al. 2011), i.e., values of  $A_{\text{flux}} = 1.110 \pm 0.070$  and  $1.070 \pm 0.050$ ; and  $A_{\text{spec}} = 0.2160 \pm 0.1060$ ,  $0.1450 \pm 0.059$ , respectively. The unmasked, resampled spectrum of W13–18 has asymmetry values of  $A_{\text{flux}} = 1.12 \pm 0.13$ , and  $A_{\text{spec}} = 0.296 \pm 0.091$ , in agreement with those for the masked resampled spectrum ( $A_{\text{flux}} = 1.14 \pm 0.13$  and  $A_{\text{spec}} = 0.272 \pm 0.097$ ). Figure 5 compares these values using the unmasked resampled spectrum for W13–18.

For  $A_{\text{flux}}$  the W13–18 value differs from the FRB hosts examined by Michałowski (2021) by  $1.31\text{--}2.96\sigma$ , and for  $A_{\text{spec}}$ ,  $2.36\text{--}2.86\sigma$ , not quite sufficient to conclusively state W13–18 does not show the same level of asymmetry as the previous hosts. W13–18 is within  $0.36\sigma$  and  $1.39\sigma$  of the mean of the LVHIS and HALOGAS asymmetry values ( $A_{\text{flux}}$  and  $A_{\text{spec}}$ , respectively). The two FRBs examined by Michałowski (2021), meanwhile, diverge from those H I surveys by  $2.03\text{--}8.69\sigma$  and  $2.78\text{--}6.22\sigma$ , again in  $A_{\text{flux}}$  and  $A_{\text{spec}}$ , respectively.

In addition to the H I global spectrum asymmetries, it is possible to calculate the 2D asymmetry,  $A_{2D}$ , using the technique of Conselice et al. (2000) and Conselice (2003), which has been applied in previous studies (e.g., Holwerda et al. 2011) to determine the galaxy merger fraction. The 2D equation is the same as Equation (7) for  $A_{\text{spec}}$ , except the flipping is done in two dimensions and the rotation point is the center of the galaxy. Using a center point of (22.3, 17.1) pixels



**Figure 5.** Comparison of  $A_{\text{flux}}$  (left panel) and  $A_{\text{spec}}$  (right panel) for W13–18 with the two FRBs presented in Michałowski (2021; red and yellow, respectively). We include the two GRB hosts (green) and the asymmetry values for the the LVHIS and HALOGAS HI surveys from Reynolds et al. (2020; black) as in Figure 3 of Michałowski (2021).

on the moment 0 map yields a value of  $A_{2D} = 0.23$ , which is significantly lower than  $A_{\text{spec}}$ , but not surprising given the low resolution of the observations (see Figure 12 of Giese et al. 2016).

It is important to consider the effects of noise on both  $A_{\text{spec}}$  and  $A_{2D}$ . These are channel-by-channel and pixel-by-pixel measurements, so noise fluctuations will increase the asymmetry measurement. Noise can also contribute to the lopsidedness measured, but since it is an integrated quantity, the effect of noise is decreased (see Figure 3 and Section 3.2 of Deg et al. 2020, where a Monte Carlo simulation was performed to explore the effects of the S/N on the measured asymmetry statistics). Thus, the “true” level of asymmetry that can be attributed to the galaxy itself rather than from the noise is lower than our values of  $A_{\text{spec}} = 0.296$  and  $A_{2D} = 0.23$ .

The mean velocity field for W13–18 (left panel of Figure 3) does not appear to be symmetric, which could be attributed to a warp in the outer disk of W13–18. The outer edges of the velocity field do not have a smooth gradient, particularly on the higher-velocity end. The beam size is larger than those high-velocity features and taking into account our limited S/N, we are hence unable to draw any firm conclusions from the velocity field alone.

Wong et al. (2016) argued that self-regulated or secular star formation within disk galaxies across five orders of magnitude in stellar mass can be governed by a constant, marginally stable

disk model. For a galaxy with a  $V_{\text{max}}$  of  $\sim 100 \text{ km s}^{-1}$ , this model predicts an SFR of  $1.3 M_{\odot} \text{ yr}^{-1}$ . This is a factor of  $\sim 2$  lower than the mid-infrared (MIR) and radio continuum SFR (albeit in agreement within  $1\sigma$  of  $\text{SFR}_{\text{radio}}$  following subtraction of the unresolved core emission), in agreement with the NUV SFR, and higher than the optical SFR in the past 30 yr by almost a factor of 3. The nearest WALLABY source to W13–18 is 16.5 Mpc away (down to a  $M_{\text{HI}}$  sensitivity of  $2.4 \times 10^9 M_{\odot}$ ), suggesting that this host galaxy is relatively isolated in HI.

What does it mean for the FRB progenitor? For the previous FRB host galaxies detected in HI, the characteristics of their HI spectra and intensity maps were attributed to merger/interaction events. However, noting the limitations of the WALLABY data, our HI data products for W13–18 do not allow us to decide for or against the hypothesis of a galaxy interaction or merger occurring, which would lead to a recent increase in star formation and the creation of an FRB progenitor (in the form of a massive star). We note that HI asymmetry does not always correspond to a galaxy merger or interaction; internal processes such as AGN or starburst feedback can also be a potential cause (Sancisi et al. 2008; Fraternali 2017). Minor mergers are also not always evident in HI spectra or intensity maps.

We stress that the inability to currently determine a high or low HI asymmetry does not necessarily argue against a fast



FRB channel model for this FRB progenitor. For instance, the FRB localization is *not inconsistent* with a spiral arm, which is generally a region of higher active star formation that could possibly be the source of a fast FRB channel progenitor. Furthermore, the high HI-to-stellar mass ratio observed for the host galaxy, the slight stellar overdensity to the northwest, and the warped velocity field could suggest a minor merger event that could trigger a fast FRB channel for the progenitor. This scenario supports the hypothesis of Michałowski (2021) where the delay between the birth of the progenitor (e.g., a massive star) and the FRB emission is 10–100 Myr, rather than billions of years. However, if such a galaxy interaction event had occurred, it is not strongly reflected in the other HI properties of W13–18, especially compared to the FRB host galaxies presented in Michałowski (2021), Kaur et al. (2022) or Lee-Waddell et al. (2023). Ultimately, a larger sample of localized FRBs with corresponding host galaxy HI information will be required in order to ascertain definitively the extent to which FRBs are associated with merger-driven star formation.

#### 4. Conclusions

We present the commensal detection of HI alongside the localization for FRB 20211127I to W13–18 through a collaboration between the CRAFT and WALLABY surveys. W13–18 has an HI mass of  $6.5 \pm 1.3 \times 10^9 M_{\odot}$ . Despite the high HI-to-stellar mass ratio of 2.17, and a possible warp in the HI velocity field, we see no strong disturbances in the HI intensity map, with the only notable feature possibly attributed to noise. The HI intensity map would benefit from an improved S/N and spatial resolution, but we nonetheless report the 1D and 2D asymmetry values, which are  $1.31$ – $2.96\sigma$  lower than the FRBs studied in Michałowski (2021) in  $A_{\text{flux}}$ , and  $2.36$ – $2.86\sigma$  lower in  $A_{\text{spec}}$ . Higher S/N and spatial resolution HI observations are required to investigate this FRB host galaxy better.

It is important to remember that W13–18 is only the fifth (and most distant) case of HI emission associated with an external galaxy hosting an FRB. We are still working with low number statistics and are currently treating each detection individually. With a larger sample size, it could be possible that we find convincing examples of nonasymmetric HI or find that disturbed HI profiles and intensity maps are the norm for FRB hosts. As localizations of FRB emission by CRAFT rapidly increase (to  $\sim 1$  per two days) and as HI emission surveys such as WALLABY progress, the sample of HI galaxies that host FRBs should also increase to the point required for a meaningful statistical study (from extragalactic HI surveys with ASKAP, we predict  $\sim 5$  new HI detections a year as commensally discovered CRAFT FRB host galaxies, not including follow-up studies with other telescopes). Such HI properties for future FRBs can also be used to probe the recent history of the host galaxy, where the star formation history is not available at the time of the FRB detection and localization.












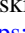



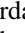
We thank the referee for useful feedback that has improved this paper. We thank Barbara Catinella, Ronald Ekers, Pascal Elahi, Karl Glazebrook, Kelley Hess, Clancy James, Dane Kleiner, Ángel R. López-Sánchez, Elizabeth Mahony, Gerhard Meurer, Tom Oosterloo, Javi Román, Lister Staveley-Smith, and Lourdes Verdes-Montenegro for useful discussions and feedback on the paper. M.G. is supported by the Australian Government through the Australian Research Council’s

Discovery Projects funding scheme (DP210102103). L.M. acknowledges the receipt of an MQ-RES scholarship from Macquarie University. R.M.S. acknowledges support from the Australian Research Council Future Fellowship FT190100155. S.B. is supported by a Dutch Research Council (NWO) Veni Fellowship (VI.Veni.212.058). A.B. acknowledges support from the Centre National d’Etudes Spatiales (CNES), France. J.X.P., as a member of the Fast and Fortunate for FRB Follow-up team, acknowledges support from NSF grants AST-1911140 and AST-1910471.

This scientific work uses data obtained from Inyarrimanha Ilgari Bundara, the CSIRO Murchison Radio-astronomy Observatory. We acknowledge the Wajarri Yamaji People as the Traditional Owners and native title holders of the Observatory site. CSIRO’s ASKAP radio telescope is part of the Australia Telescope National Facility (<https://ror.org/05qajvd42>). Operation of ASKAP is funded by the Australian Government with support from the National Collaborative Research Infrastructure Strategy. ASKAP uses the resources of the Pawsey Supercomputing Research Centre. Establishment of ASKAP, Inyarrimanha Ilgari Bundara, the CSIRO Murchison Radio-astronomy Observatory and the Pawsey Supercomputing Research Centre are initiatives of the Australian Government, with support from the Government of Western Australia and the Science and Industry Endowment Fund. We also thank the MRO site staff. This research has made use of the NASA/IPAC Extragalactic Database (NED) which is operated by the Jet Propulsion Laboratory, California Institute of Technology, under contract with the National Aeronautics and Space Administration. Parts of this research were supported by the Australian Research Council Centre of Excellence for All Sky Astrophysics in 3 Dimensions (ASTRO 3D), through project number CE170100013. This research is based on observations collected at the European Southern Observatory under ESO program 0105.A-0687(C) (PI: J.-P. Macquart). We acknowledge support from the Australian SKA Regional Centre (AusSRC).

The stellar mass and associated SFR measures are based on observations obtained at the Southern Astrophysical Research (SOAR) telescope, which is a joint project of the Ministério da Ciência, Tecnologia e Inovações do Brasil (MCTI/LNA), the US National Science Foundation’s NOIRLab, the University of North Carolina at Chapel Hill (UNC), and Michigan State University (MSU).

#### ORCID iDs

M. Glowacki  <https://orcid.org/0000-0002-5067-8894>  
 K. Lee-Waddell  <https://orcid.org/0000-0003-4844-8659>  
 A. T. Deller  <https://orcid.org/0000-0001-9434-3837>  
 A. C. Gordon  <https://orcid.org/0000-0002-5025-4645>  
 J. A. Grundy  <https://orcid.org/0000-0002-4440-8046>  
 L. Marnoch  <https://orcid.org/0000-0003-1483-0147>  
 S. D. Ryder  <https://orcid.org/0000-0003-4501-8100>  
 R. M. Shannon  <https://orcid.org/0000-0002-7285-6348>  
 O. I. Wong  <https://orcid.org/0000-0003-4264-3509>  
 H. Dénes  <https://orcid.org/0000-0002-9214-8613>  
 B. S. Koribalski  <https://orcid.org/0000-0003-4351-993X>  
 J. Rhee  <https://orcid.org/0000-0001-8496-4306>  
 S. Bhandari  <https://orcid.org/0000-0003-3460-506X>  
 A. Bosma  <https://orcid.org/0000-0002-1128-6089>  
 B. W. Holwerda  <https://orcid.org/0000-0002-4884-6756>  
 J. X. Prochaska  <https://orcid.org/0000-0002-7738-6875>

## References

- Bannister, K. W., Shannon, R. M., Macquart, J. P., et al. 2017, *ApJL*, **841**, L12
- Bannister, K. W., Deller, A. T., Phillips, C., et al. 2019, *Sci*, **365**, 565
- Bhandari, S., Heintz, K. E., Aggarwal, K., et al. 2022, *AJ*, **163**, 69
- Catinella, B., Saintonge, A., Janowiecki, S., et al. 2018, *MNRAS*, **476**, 875
- Chynoweth, K. M., Langston, G. I., Yun, M. S., et al. 2008, *AJ*, **135**, 1983
- Cluver, M. E., Jarrett, T. H., Dale, D. A., et al. 2017, *ApJ*, **850**, 68
- Cluver, M. E., Jarrett, T. H., Hopkins, A. M., et al. 2014, *ApJ*, **782**, 90
- Conselice, C. J. 2003, *ApJS*, **147**, 1
- Conselice, C. J., Bershadsky, M. A., & Jangren, A. 2000, *ApJ*, **529**, 886
- Cordes, J. M., & Chatterjee, S. 2019, *ARA&A*, **57**, 417
- Day, C. K., Deller, A. T., Shannon, R. M., et al. 2020, *MNRAS*, **497**, 3335
- Deboer, B. D. R., Gough, R. G., Bunton, J. D., et al. 2009, *Proc. IEEE*, **97**, 1507
- Deg, N., Blyth, S. L., Hank, N., Kruger, S., & Carignan, C. 2020, *MNRAS*, **495**, 1984
- Deg, N., Spekkens, K., Westmeier, T., et al. 2022, *PASA*, **39**, e059
- Di Teodoro, E. M., & Fraternali, F. 2015, *MNRAS*, **451**, 3021
- Espada, D., Verdes-Montenegro, L., Huchtmeier, W. K., et al. 2011, *A&A*, **532**, A117
- Fraternali, F. 2017, in *Gas Accretion onto Galaxies, Astrophysics and Space Science Library*, Vol. 430, ed. A. Fox & R. Davé (Cham: Springer), 323
- Giese, N., van der Hulst, T., Serra, P., & Oosterloo, T. 2016, *MNRAS*, **461**, 1656
- Glowacki, M., Deg, N., Blyth, S. L., et al. 2022, *MNRAS*, **517**, 1282
- Gordon, A. C., Fong, W.-f., Kilpatrick, C. D., et al. 2023, arXiv:2302.05465
- Grundy, J. A., Wong, O. I., Lee-Waddell, K., et al. 2023, *PASA*, **40**, e012
- Hale, C. L., Robotham, A. S. G., Davies, L. J. M., et al. 2019, *MNRAS*, **487**, 3971
- Haynes, M. P., Hogg, D. E., Maddalena, R. J., Roberts, M. S., & van Zee, L. 1998, *AJ*, **115**, 62
- Heald, G., Józsa, G., Serra, P., et al. 2011, *A&A*, **526**, A118
- Holwerda, B. W., Pirzkal, N., Cox, T. J., et al. 2011, *MNRAS*, **416**, 2426
- Hsu, T.-Y., Hashimoto, T., Hatsukade, B., et al. 2023, *MNRAS*, **519**, 2030
- Huynh, M., Dempsey, J., Whiting, M. T., & Ophel, M. 2020, in *ASP Conf. Ser. 522, Astronomical Data Analysis Software and Systems XXVII*, ed. P. Ballester et al. (San Francisco, CA: ASP), 263
- James, C. W., Ghosh, E. M., Prochaska, J. X., et al. 2022, *MNRAS*, **516**, 4862
- Jarrett, T. H., Chester, T., Cutri, R., et al. 2000, *AJ*, **119**, 2498
- Jarrett, T. H., Cohen, M., Masci, F., et al. 2011, *ApJ*, **735**, 112
- Johnson, B. D., Leja, J., Conroy, C., & Speagle, J. S. 2021, *ApJS*, **254**, 22
- Jones, D. H., Read, M. A., Saunders, W., et al. 2009, *MNRAS*, **399**, 683
- Kalberla, P. M. W., & Kerp, J. 2009, *ARA&A*, **47**, 27
- Kaur, B., Kanekar, N., & Prochaska, J. X. 2022, *ApJL*, **925**, L20
- Koribalski, B. S., Staveley-Smith, L., Westmeier, T., et al. 2020, *Ap&SS*, **365**, 118
- Koribalski, B. S., Wang, J., Kamphuis, P., et al. 2018, *MNRAS*, **478**, 1611
- Lee-Waddell, K., James, C. W., Ryder, S. D., et al. 2023, *PASA*, submitted
- Lee-Waddell, K., Spekkens, K., Chandra, P., et al. 2016, *MNRAS*, **460**, 2945
- Lorimer, D. R., Bailes, M., McLaughlin, M. A., Narkevic, D. J., & Crawford, F. 2007, *Sci*, **318**, 777
- Macquart, J.-P., Bailes, M., Bhat, N. D. R., et al. 2010, *PASA*, **27**, 272
- Macquart, J. P., Prochaska, J. X., McQuinn, M., et al. 2020, *Natur*, **581**, 391
- Mahony, E. K., Ekers, R. D., Macquart, J.-P., et al. 2018, *ApJL*, **867**, L10
- Masters, K. L., Crook, A., Hong, T., et al. 2014, *MNRAS*, **443**, 1044
- McMahon, R. G., Banerji, M., Gonzalez, E., et al. 2013, *Msngr*, **154**, 35
- Meurer, G. R., Hanish, D. J., Ferguson, H. C., et al. 2006, *ApJS*, **165**, 307
- Meyer, M., Robotham, A., Obreschkow, D., et al. 2017, *PASA*, **34**, 52
- Meyer, M. J., Zwaan, M. A., Webster, R. L., Schneider, S., & Staveley-Smith, L. 2008, *MNRAS*, **391**, 1712
- Michałowski, M. J. 2021, *ApJL*, **920**, L21
- Molnár, D. C., Sargent, M. T., Leslie, S., et al. 2021, *MNRAS*, **504**, 118
- Planck Collaboration, Ade, P. A. R., Aghanim, N., et al. 2016, *A&A*, **594**, A13
- Reynolds, T. N., Westmeier, T., Staveley-Smith, L., et al. 2019, *MNRAS*, **482**, 3591
- Reynolds, T. N., Westmeier, T., Staveley-Smith, L., Chauhan, G., & Lagos, C. D. P. 2020, *MNRAS*, **493**, 5089
- Richter, O. G., & Sancisi, R. 1994, *A&A*, **290**, L9
- Sancisi, R., Fraternali, F., Oosterloo, T., & van der Hulst, T. 2008, *A&ARv*, **15**, 189
- Schiminovich, D., Wyder, T. K., Martin, D. C., et al. 2007, *ApJS*, **173**, 315
- Scott, D. R., Cho, H., Day, C. K., et al. 2023, arXiv:2301.13484
- Serra, P., Westmeier, T., Giese, N., et al. 2015, *MNRAS*, **448**, 1922
- Westmeier, T., Deg, N., Spekkens, K., et al. 2022, *PASA*, **39**, e058
- Westmeier, T., Kitaëff, S., Pallot, D., et al. 2021, *MNRAS*, **506**, 3962
- Whiting, M. T. 2020, in *ASP Conf. Ser. 522, Astronomical Data Analysis Software and Systems XXVII*, ed. P. Ballester et al. (San Francisco, CA: ASP), 469
- Wong, O. I., Meurer, G. R., Zheng, Z., et al. 2016, *MNRAS*, **460**, 1106
- Wright, E. L., Eisenhardt, P. R. M., Mainzer, A. K., et al. 2010, *AJ*, **140**, 1868